

Constraining ultralight scalar dark matter couplings with the European Pulsar Timing Array second data release

Yu-Mei Wu^{1,2,3,*} and Qing-Guo Huang^{2,4,3,†}

¹*Center for Gravitation and Cosmology, College of Physical Science and Technology, Yangzhou University, Yangzhou, 225009, China*

²*School of Fundamental Physics and Mathematical Sciences, Hangzhou Institute for Advanced Study, UCAS, Hangzhou 310024, China*

³*School of Physical Sciences, University of Chinese Academy of Sciences, No. 19A Yuquan Road, Beijing 100049, China*

⁴*CAS Key Laboratory of Theoretical Physics, Institute of Theoretical Physics, Chinese Academy of Sciences, Beijing 100190, China*

Pulsar Timing Arrays (PTAs) offer an independent method for searching for ultralight dark matter (ULDM), whose wavelike nature induces periodic oscillations in the arrival times of radio pulses. In addition to this gravitational effect, the direct coupling between ULDM and ordinary matter results in pulsar spin fluctuations and reference clock shifts, leading to observable effects in PTAs. The second data release from the European PTA (EPTA) indicates that ULDM cannot account for all dark matter in the mass range $m_\phi \in [10^{-24.0}, 10^{-23.3}]$ eV based solely on gravitational effects. In this work, we derive constraints on the coupling coefficients by considering both gravitational and coupling effects. Our results demonstrate that EPTA provides stronger constraints on these couplings than previous PTA experiments, and it establishes similar or even tighter constraints compared to other precise experiments, such as atomic clock experiments.

I. INTRODUCTION

The existence of dark matter has been confirmed by numerous experiments, including galaxy rotation curves [1, 2], velocity dispersions [3], and gravitational lensing [4]. Additionally, observations of the cosmic microwave background suggest that dark matter constitutes roughly five times more of the universe’s mass than visible matter [5], according to the widely accepted Lambda cold dark matter paradigm. However, The fundamental nature of dark matter, including its composition and interaction with the Standard Model, is still a mystery. Among the many candidates for cold dark matter, weakly interacting massive particles (WIMPs) were initially highly anticipated, yet extensive searches have so far yielded no positive results [6]. Moreover, traditional CDM candidates encounter challenges on small scales, such as the discrepancy between predictions of steep central densities in galaxy cores and observed flatter density profiles (the cusp-core problem, [7, 8]), as well as the mismatch between the predicted steep increase in the number of low-mass subhalos and the significantly lower number of observed satellites around the galaxies (the missing satellite problem, [9, 10]). One potential solution to these issues is the hypothesis that dark matter consists of ultralight bosons [11], typically with mass $m_\phi \ll 10^{-6}$ eV, whose large de Broglie wavelength can efficiently suppress structure formation on small scales [12].

The phenomenon of ultralight dark matter (ULDM) encompasses a broad range of possibilities, allowing it to be constrained by various observational data. For

example, measurements of the cosmic microwave background (CMB) exclude ULDM with masses below $m_\phi < 10^{-24}$ eV [13]. Dwarf galaxy dynamics [14] provide a stronger lower bound at $m_\phi > 10^{-22}$ eV, while galaxy rotation curves [15] and Lyman- α forest observations [16] further tighten this limit to $m_\phi > 10^{-21}$ eV. However, these constraints from non-CMB experiments are heavily reliant on models of small-scale structure formation [17, 18], which introduce considerable uncertainties. To overcome these uncertainties, it is crucial to employ complementary methods that can provide independent constraints on ULDM in this mass range. One promising approach involves pulsar timing arrays (PTAs), which monitor the highly regular radio pulses of millisecond pulsars over extended periods [19–21]. As sensitive detectors operating in the nanohertz frequency range, PTAs offer a feasible means to detect or constrain ULDM with masses between 10^{-24} eV and 10^{-20} eV.

ULDM can generate detectable signals in PTAs through two primary mechanisms. First, the oscillations of ULDM can directly induce spacetime fluctuations, resulting in changes to the times of arrival (ToAs) of radio pulses [22–24], known as timing residuals—the differences between the actual measured and predicted ToAs. This phenomenon is referred to as the gravitational effect of ULDM. Second, ULDM may interact with the Standard Model, and its coupling with the pulsars and the Earth, both composed of ordinary matter, can leave observable imprints on the ToAs in a more subtle manner [25–27]. This interaction is referred to as the coupling effect. Several studies have explored ULDM using PTA datasets, but the gravitational and coupling effects are typically considered in isolation [25, 28–31]. Furthermore, analyses of the coupling effect often assume that ultralight fields constitute the entirety of dark matter. However, two critical points warrant emphasis. First, the gravitational ef-

* wuyumei@yzu.edu.cn

† Corresponding author: huangqg@itp.ac.cn

fect of ULDM is always present, regardless of any potential interaction with the Standard Model. Second, recent constraints on ULDM density, derived solely from the gravitational effect using data from the European PTA second data release (EPTA DR2), have ruled out the possibility that ultralight particles constitute 100% of the local dark matter within the mass range of $[10^{-24}, 10^{-23.3}]$ eV [30]. This underscores the importance of considering both effects in the analyses of coupling constraints.

In this paper, we adopt a more comprehensive approach by simultaneously considering both the gravitational and coupling effects based on EPTA DR2, and we present updated constraints for the ULDM couplings derived from this unified analysis. The structure of this work is as follows: Sec. II introduces the observable pulsar timing effects induced by scalar dark matter, Sec. III provides details of our data analysis, while Sec. IV present the results and conclusions.

II. GRAVITATIONAL EFFECT AND COUPLING EFFECT FROM SCALAR DARK MATTER

In this section, we provide a brief overview of the timing signal induced by scalar field dark matter, focusing on both the gravitational and coupling effects. For a more detailed derivation, one can refer to [22, 27].

On the galactic scale, the spacetime can be approximately described by Minkowski. The Lagrangian of a free scalar dark matter field with mass m_ϕ is

$$L_\phi = \frac{1}{2}\partial^\mu\phi\partial_\mu\phi - \frac{1}{2}m_\phi^2\phi^2. \quad (1)$$

As the characteristic speed of the dark matter is non-relativistic $v \sim 10^{-3}$, and the occupation number of the scalar field is huge, the ultralight scalar dark matter can be described as a monochromatic classical wave,

$$\phi(\mathbf{x}, t) = A\hat{\phi}(\mathbf{x})\cos(2\pi ft + \alpha(\mathbf{x})), \quad (2)$$

where the overall oscillation amplitude A is related to the energy density of the scalar field ρ_ϕ , the oscillation frequency f is determined by the particle mass m_ϕ ,

$$A = \frac{\sqrt{2\rho_\phi}}{m_\phi}, \quad f = \frac{m_\phi}{2\pi}, \quad (3)$$

$\alpha(\mathbf{x})$ is the position-dependent phase, and the additional random factor $\hat{\phi}(\mathbf{x})$ is introduced to capture the stochastic behavior when accounting for the interference among the field modes with different frequencies due to the small velocity dispersion [32].

The oscillating scalar field would contribute to a time-dependent tensor-momentum tensor, which induces a gravitational potential perturbation to the flat background. The radio pulse travel from the pulsar to the

Earth would experience a redshift and hence a delay on the arrival time,

$$\Delta t_{grav} = \frac{\Phi_c}{2m_\phi} \left[\hat{\phi}_E^2 \sin(2m_\phi t + 2\gamma_E) - \hat{\phi}_P^2 \sin(2m_\phi t + 2\gamma_P) \right], \quad (4)$$

which is referred to the gravitational effect of ULDM. Here, Φ_c is the amplitude of oscillating gravitational potential,

$$\Phi_c = \frac{\pi G \rho_\phi}{m_\phi^2} \approx 6.1 \times 10^{-18} \left(\frac{m_\phi}{10^{-22} \text{eV}} \right)^{-2} \left(\frac{\rho_\phi}{\rho_0} \right), \quad (5)$$

with $\rho_0 = 0.4 \text{ GeV/cm}^3$ denoting the local DM density, $\hat{\phi}_E = \hat{\phi}(\mathbf{x}_E)$ and $\hat{\phi}_P = \hat{\phi}(\mathbf{x}_P)$ are the oscillation amplitude normalized factors of the scalar field at the Earth and the pulsar, respectively, while $\gamma_E = \alpha(\mathbf{x}_E)$ and $\gamma_P = \alpha(\mathbf{x}_P) - m_\phi |\mathbf{x}_P|$ represent the redefined phases at these locations.

Apart from the gravitational effect inherent in any matter in motion, the ULDM could couple to Standard Model in a plethora of ways. The possible coupling to the QED sector and QCD sector can be parameterized as [33],

$$L_{int} = \frac{\phi}{\Lambda} \left(\frac{d_\gamma}{4e^2} F_{\mu\nu} F^{\mu\nu} - \sum_{f=e,\mu} d_f m_f \bar{f} f + \frac{d_g \beta_3}{2g_3} G_{\mu\nu}^A G_A^{\mu\nu} - \sum_{q=u,d} (d_q + \gamma_q d_g) m_q \bar{q} q \right), \quad (6)$$

where $\Lambda = M_{pl}/\sqrt{4\pi}$, with M_{pl} denoting the Planck mass. Here, $F_{\mu\nu}$ represents the electromagnetic field strength tensor, while $G_{\mu\nu}^A$ is the gauge-invariant gluon strength tensor. The QCD gauge coupling is indicated by g_3 , and β_3 refers to the beta function that governs the running of g_3 . Additionally, γ_q represents the light quark anomalous dimension, and m_f and m_q denote the masses of fermions and quarks, respectively. The d values are dimensional coupling coefficients. Through these couplings, fluctuations in the ULDM background induce variations in the fundamental constants of the Standard Model, including the electromagnetic coupling constant and the masses of electrons, muons, quarks, and nucleons,

$$\begin{aligned} \frac{\delta\alpha}{\alpha} &= \frac{d_\gamma}{\Lambda} \phi, & \frac{\delta m_{e,\mu}}{m_{e,\mu}} &= \frac{d_{e,\mu}}{\Lambda} \phi, \\ \frac{\delta m_q}{m_q} &= \frac{d_q}{\Lambda} \phi, & \frac{\delta m_{p,n}}{m_{p,n}} &= \frac{d_g + C_n d_{\hat{m}}}{\Lambda} \phi, \end{aligned} \quad (7)$$

where $C_n = 0.048$, and $d_{\hat{m}}$ is a symmetric combination of the quark mass coupling $d_{\hat{m}} = (d_u m_u + d_d m_d)/(m_u + m_d)$.

The timing residuals resulting from fluctuations in fundamental constants arise from two main aspects. First, shifts in particle mass lead to variations in the pulsar's moment of inertia, which in turn cause fluctuations in

the pulsar’s spin frequency by the conservation of angular momentum. Second, the atomic clock on Earth, used to measure the ToAs of radio pulses, also experiences frequency shifts, contributing to the observed timing residuals. Overall, the timing residuals induced by the coupling effect, stemming from both pulsar spin fluctuations and shifts in the Earth’s atomic clock, are expressed as:

$$\Delta t_{\text{coupl}} = \frac{A_i}{m_\phi} \left[y_P^i \hat{\phi}_P \sin(m_\phi t + \gamma_P) + y_E^i \hat{\phi}_E \sin(m_\phi t + \gamma_E) \right], \quad (8)$$

where $A_i = d_i \sqrt{2\rho_\phi} / (m_\phi \Lambda)$, y_P and y_E respectively parameterize the pulsar or the the atomic clock sensitivity to a specific coupling and are specifically given by

$$\begin{aligned} y_P^g &= -5, & y_P^{\hat{m}} &= -0.24, & y_P^\gamma &= 0, \\ y_P^\mu &= 2 \times 10^{-3}, & y_P^e &= 1.7 \times 10^{-5}; \\ y_E^g &= 1, & y_E^{\hat{m}} &= 0.296, & y_E^\gamma &= 4.83, \\ y_E^\mu &= 0, & y_E^e &= 2. \end{aligned} \quad (9)$$

III. DATA ANALYSIS

We employ the EPTA DR2 dataset to constrain the coupling effect of ULDM. This dataset includes observational data from 25 pulsars, covering a total observation period of 24.7 years [34]. The official EPTA collaboration has previously utilized this dataset to investigate the gravitational effect of ULDM [30], and we will adopt a similar methodology in our analyses.

The expected arrival times of radio pulses for each individual pulsar are described by a timing model that incorporates various pulsar characteristics, such as its position in the sky, spin-down rate, and proper motion. Timing residuals are obtained by subtracting these expected arrival times from the actual observed times. These residuals arise from several contributing factors, including inaccuracies in the timing model, stochastic noise during the generation and propagation of the radio pulses, and the potential astrophysical signals of interest that we aim to detect. The timing models for each pulsar are included with the dataset. To effectively extract the desired signals, a comprehensive analysis of the noise present in the data is essential.

The stochastic noise specific to each pulsar can be classified into two categories: time-uncorrelated white noise and time-correlated red noise. White noise accounts for measurement uncertainties and other potential time-independent errors, which may arise from factors such as instrumental miscalibration and changes in pulse profiles [35, 36]. This white noise is modeled using two parameters: “EFAC,” which scales the ToA uncertainties, and “EQUAD,” an additional term incorporated in quadrature. In contrast, red noise includes achromatic spin noise intrinsic to each pulsar, resulting from rotational instabilities [37], as well as chromatic dispersion variations occurring as radio pulses traverse the interstellar medium [38]. Red noise is typically modeled by

a power-law spectrum characterized by two parameters: the amplitude A_{red} and the spectral index γ_{red} . Furthermore, in the search for stochastic gravitational-wave background (SGWB), while the critical detection criterion—the distinctive Hellings-Downs quadrupole correlation—has not yet yielded strong evidence, a common uncorrelated spectrum across all pulsars, likely arising from the auto-correlation component of the SGWB, has shown considerable promise [39]. Therefore, we will also incorporate the contribution of this common uncorrelated red noise when modeling the timing residuals.

The signals from ULDM, arising from both the gravitational and coupling effects, are described by Eq. (4) and Eq. (8) as deterministic sinusoidal functions, characterized by amplitude parameters Φ_c and A_i , amplitude normalized factors $\hat{\phi}_E$ and $\hat{\phi}_P$, mass (or frequency) parameter m_ϕ , and phase parameters γ_E and γ_P . For scales smaller than the de Broglie wavelength $l \sim 0.4 \text{ kpc} (10^{-22} \text{ eV}/m_\phi)$, the ULDM scalar field demonstrates coherent oscillations with a consistent amplitude factor $\hat{\phi}$. Given that the typical distances between pulsars and between the pulsars and Earth are comparable to this coherence length, we consider two representative scenarios: “Correlated,” where the Earth and all pulsars share the same normalized amplitude factor ($\hat{\phi}_E = \hat{\phi}_P$), and “Uncorrelated,” where the Earth and pulsars have independent factors. To facilitate a more flexible search for or constraint on ULDM signals, we partition the mass range $m_\phi \in [10^{-24}, 10^{-22}] \text{ eV}$ into equally spaced small segments. Additionally, since ULDM cannot exceed the total dark matter density (i.e., $\rho_\phi < \rho_0$), we impose an upper limit Φ_0 on the amplitude Φ_c .

The analysis of PTA data begins with a thorough examination of the noise for each individual pulsar. We then fix the white noise at their maximum likelihood values to reduce the computational cost. The red noises, which can be specific to individual pulsars or common across all pulsars, are modeled simultaneously with the target signal. All relevant parameters and their associated priors are outlined in Table 1. We will utilize Bayesian methodology to assess the presence or absence of the signal by calculating the Bayes factor \mathbf{BF} between the “noise + signal” model and the “noise only” model. A positive indication of the signal’s presence can be declared when $\ln \mathbf{BF} > 3$. If no signal is detected, we will estimate the 95% upper limit for the amplitude. To evaluate the likelihood, we utilize the `enterprise` [40] and `enterprise_extension` [41] packages, applying the product-space method [42–44] to compute the Bayes factor. For parameter estimation, we implement Markov-chain Monte Carlo sampling using the `PTMCMCSampler` package [45].

TABLE I. Parameters and their prior distributions used in the analyses. "U" and "log-U" denote uniform and log-uniform distributions, respectively. "One parameter for PTA" indicates that the parameter is shared across the entire data set, while "one parameter per pulsar" signifies that the parameter varies from pulsar to pulsar.

Parameter	description	prior	comments
White noise			
E_k	EFAC per backend/receiver system	U[0, 10]	single-pulsar analysis only
Q_k [s]	EQUAD per backend/receiver system	log-U[-8.5, -5]	single-pulsar analysis only
Red noise (including SN and DM)			
\mathcal{A}_{RN}	Red-noise power-law amplitude	log-U[-20, -8]	one parameter per pulsar
γ_{RN}	red-noise power-law index	U[0, 10]	one parameter per pulsar
Common noise			
\mathcal{A}_{GWB}	common-noise power-law amplitude	log-U[-20, -6]	one parameter for PTA
Ultralight dark matter signal			
Φ_c	ULDM gravitational effect amplitude	log-U[-20, $\log_{10} \Phi_0$]	one parameter for PTA
A_i	ULDM coupling effect amplitude	log-U[-20, -10]	one parameter for PTA
m_ϕ	ULDM mass	log-U[-24, -22]	one parameter for PTA
$\hat{\phi}_E^2$	Earth normalized signal amplitude	e^{-x}	one parameter for PTA
$\hat{\phi}_P^2$	Pulsar normalized signal amplitude	e^{-x}	one parameter per pulsar
γ_E	oscillation phase on Earth	U[0, 2π]	one parameter for PTA
γ_P	equivalent oscillation phase on pulsar	U[0, 2π]	one parameter per pulsar

IV. RESULTS AND DISCUSSION

In our analysis of the coupling effect described by Eq. (8), we consider the induced timing signals from individual couplings with the photon (d_γ), electron (d_e), muon (d_μ), gluon (d_g), and quark (d_q) separately, alongside the ubiquitous gravitational effect outlined in Eq. (4). Within the mass range we explore, $10^{-24}\text{eV} < m_\phi < 10^{-22}\text{eV}$, we found no positive evidence for the ULDM signal, as indicated by $\ln \mathbf{BF} < 1$. Consequently, we compute constraints on the ULDM coupling constants. It is important to note that the amplitude parameters A_i encompass both the coupling constants d_i and the ULDM density ρ_ϕ ; thus, we can only derive upper limits for the product $d_i\sqrt{\rho_\phi}$ based on the 95th percentile of the marginalized posterior distributions of A_i . The results of these constraints are presented in Fig. 1.

The constraints on individual coupling constants from the ULDM coupling effect are displayed in each panel for both "Correlated" and "Uncorrelated" scenarios, represented by solid lines. It is worth noting that the parameters d_γ and d_e couple significantly more strongly to the Earth term than to the pulsar term, resulting in minimal differences between the "Correlated" and "Uncorrelated" cases. For comparison, we also include other experimental constraints, indicated by dashed lines. Our findings reveal that PTA experiments are slightly less sensitive than the most precise atomic clock results [46, 51] in constraining the coupling constant d_γ , yet they are roughly comparable for d_m and exhibit greater sensitivity for d_g . Importantly, PTAs can constrain the d_e coupling, which is not feasible with atomic clock experiments due to the cancellation of the d_e dependence in the relative frequency shifts between clocks that use the same atomic transition. Furthermore, PTAs surpass Weak Equivalent

Principle constraints [48, 52] by several orders of magnitude. While there are currently no laboratory constraints on d_μ due to the scarcity of muons on Earth, neutron stars, which host a substantial number of muons, provide a more favorable environment for constraining d_μ . Consequently, PTAs are exceptionally sensitive to d_μ , enhancing the previous projected constraints from the orbital decay of a neutron star (NS) binary system [49, 50] by three orders of magnitude.

In addition, our constraints on $d_i\sqrt{\rho_\phi}$ based on EPTA DR2 are 2 \sim 3 times stricter than those from the NANOGrav collaboration's 15-year datasets [31], which is consistent with the comparison of constraints on dark matter density ρ_ϕ derived from pure gravitational effects in previous searches by both collaborations [30, 31]. This suggests that EPTA exhibits higher sensitivity to deterministic signals due to its longer observational span.

In the future, as sensitivity improves, if the dataset constrains the ULDM to a fraction f_ϕ of the total dark matter abundance, the constraints on the coupling coefficients d_i could tighten by a factor of $\sqrt{f_\phi}$. Additionally, it may become possible to detect a sinusoidal monochromatic signal in PTAs. However, such a signal could originate from various sources, including the ULDM gravitational effect, the ULDM coupling effect, or a continuous gravitational wave. In this case, we will need to utilize the correlation of signals between pulsars to resolve their degeneracy [27, 53, 54].

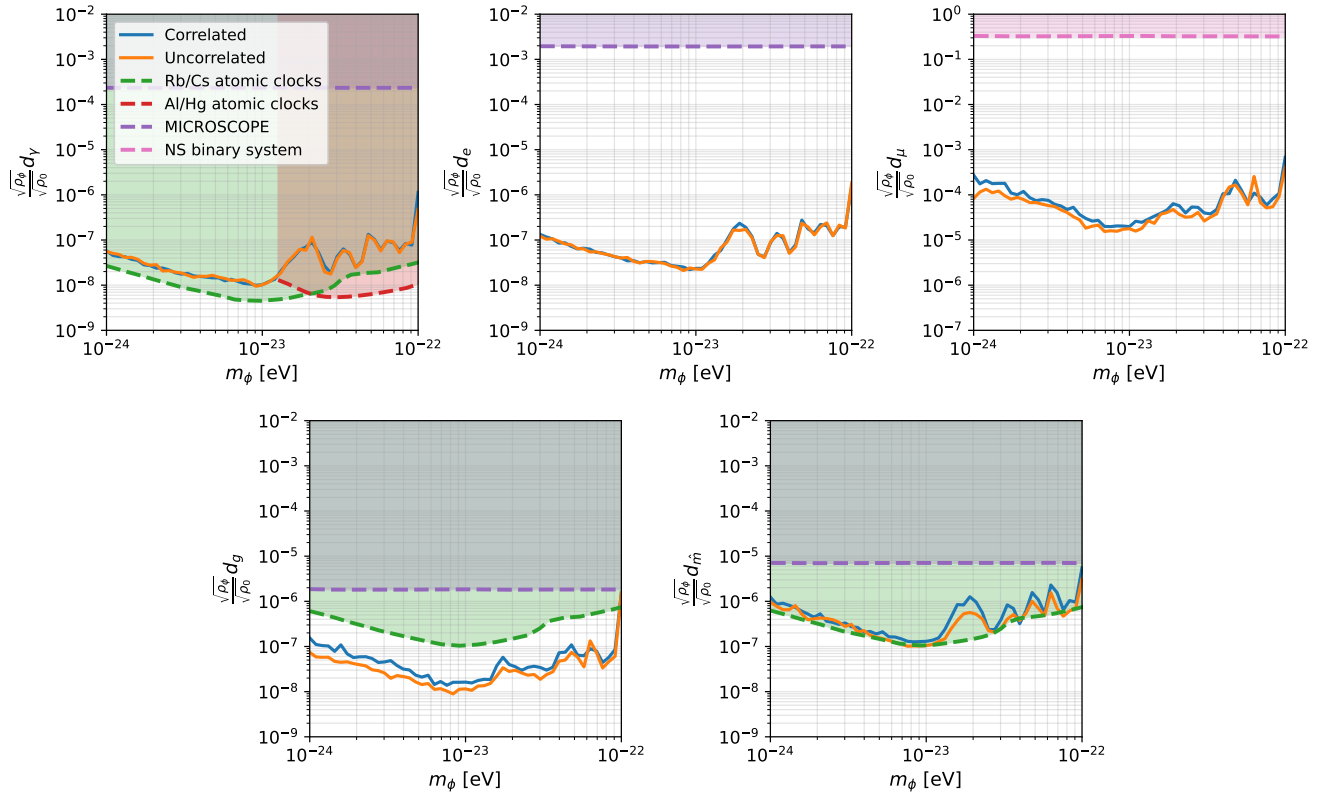


FIG. 1. Upper limits on the five dimensionless parameters $d_i \sqrt{\rho_\phi} / \sqrt{\rho_0}$ (solid lines) as a function of mass, derived from the coupling effect of the ULDM. The blue and orange solid lines represent searches for the ULDM signal in correlated and uncorrelated scenarios, respectively. Dashed lines indicate constraints from other experiments, with green, red, purple, and pink dashed lines corresponding to the “Rb/Cs atomic clocks” [46], “Al/Hg atomic clocks” [47], “MICROSCOPE” [48] and “NS binary system” [49, 50] experiments, respectively.

ACKNOWLEDGMENTS

This work is supported by the grants from NSFC (Grant No. 12250010, 11991052), Key Research Program

of Frontier Sciences, CAS, Grant No. ZDBS-LY-7009. We acknowledge the use of HPC Cluster of ITP-CAS.

-
- [1] V. C. Rubin, Jr. Ford, W. K., and N. Thonnard, “Rotational properties of 21 SC galaxies with a large range of luminosities and radii, from NGC 4605 (R=4kpc) to UGC 2885 (R=122kpc).” *Astrophys. J.* **238**, 471–487 (1980).
 - [2] V. C. Rubin, Jr. Ford, W. K., N. Thonnard, and D. Burstein, “Rotational properties of 23Sb galaxies.” *Astrophys. J.* **261**, 439–456 (1982).
 - [3] S. M. Faber and R. E. Jackson, “Velocity dispersions and mass-to-light ratios for elliptical galaxies.” *Astrophys. J.* **204**, 668–683 (1976).
 - [4] Richard Massey, Thomas Kitching, and Johan Richard, “The dark matter of gravitational lensing,” *Rept. Prog. Phys.* **73**, 086901 (2010), arXiv:1001.1739 [astro-ph.CO].
 - [5] N. Aghanim *et al.* (Planck), “Planck 2018 results. VI. Cosmological parameters,” *Astron. Astrophys.* **641**, A6 (2020), [Erratum: *Astron. Astrophys.* 652, C4 (2021)], arXiv:1807.06209 [astro-ph.CO].
 - [6] Marc Schumann, “Direct Detection of WIMP Dark Matter: Concepts and Status,” *J. Phys. G* **46**, 103003 (2019), arXiv:1903.03026 [astro-ph.CO].
 - [7] Gianfranco Gentile, P. Salucci, U. Klein, D. Vergani, and P. Kalberla, “The Cored distribution of dark matter in spiral galaxies,” *Mon. Not. Roy. Astron. Soc.* **351**, 903 (2004), arXiv:astro-ph/0403154.
 - [8] W. J. G. de Blok, “The Core-Cusp Problem,” *Adv. Astron.* **2010**, 789293 (2010), arXiv:0910.3538 [astro-ph.CO].

- [9] B. Moore, S. Ghigna, F. Governato, G. Lake, Thomas R. Quinn, J. Stadel, and P. Tozzi, “Dark matter substructure within galactic halos,” *Astrophys. J. Lett.* **524**, L19–L22 (1999), [arXiv:astro-ph/9907411](#).
- [10] Anatoly A. Klypin, Andrey V. Kravtsov, Octavio Valenzuela, and Francisco Prada, “Where are the missing Galactic satellites?” *Astrophys. J.* **522**, 82–92 (1999), [arXiv:astro-ph/9901240](#).
- [11] Wayne Hu, Rennan Barkana, and Andrei Gruzinov, “Cold and fuzzy dark matter,” *Phys. Rev. Lett.* **85**, 1158–1161 (2000), [arXiv:astro-ph/0003365](#).
- [12] Lam Hui, Jeremiah P. Ostriker, Scott Tremaine, and Edward Witten, “Ultralight scalars as cosmological dark matter,” *Phys. Rev. D* **95**, 043541 (2017), [arXiv:1610.08297 \[astro-ph.CO\]](#).
- [13] Renée Hlozek, David J. E. Marsh, and Daniel Grin, “Using the Full Power of the Cosmic Microwave Background to Probe Axion Dark Matter,” *Mon. Not. Roy. Astron. Soc.* **476**, 3063–3085 (2018), [arXiv:1708.05681 \[astro-ph.CO\]](#).
- [14] David J. E. Marsh and Jens C. Niemeyer, “Strong Constraints on Fuzzy Dark Matter from Ultrafaint Dwarf Galaxy Eridanus II,” *Phys. Rev. Lett.* **123**, 051103 (2019), [arXiv:1810.08543 \[astro-ph.CO\]](#).
- [15] Nitsan Bar, Diego Blas, Kfir Blum, and Sergey Sibiryakov, “Galactic rotation curves versus ultralight dark matter: Implications of the soliton-host halo relation,” *Phys. Rev. D* **98**, 083027 (2018), [arXiv:1805.00122 \[astro-ph.CO\]](#).
- [16] Keir K. Rogers and Hiranya V. Peiris, “Strong Bound on Canonical Ultralight Axion Dark Matter from the Lyman-Alpha Forest,” *Phys. Rev. Lett.* **126**, 071302 (2021), [arXiv:2007.12705 \[astro-ph.CO\]](#).
- [17] Hsi-Yu Schive, Ming-Hsuan Liao, Tak-Pong Woo, Shing-Kwong Wong, Tzihong Chiueh, Tom Broadhurst, and W. Y. Pauchy Hwang, “Understanding the Core-Halo Relation of Quantum Wave Dark Matter from 3D Simulations,” *Phys. Rev. Lett.* **113**, 261302 (2014), [arXiv:1407.7762 \[astro-ph.GA\]](#).
- [18] Jiajun Zhang, Jui-Lin Kuo, Hantao Liu, Yue-Lin Sming Tsai, Kingman Cheung, and Ming-Chung Chu, “The Importance of Quantum Pressure of Fuzzy Dark Matter on Lyman-Alpha Forest,” *Astrophys. J.* **863**, 73 (2018), [arXiv:1708.04389 \[astro-ph.CO\]](#).
- [19] M. V. Sazhin, “Opportunities for detecting ultralong gravitational waves,” *Soviet Ast.* **22**, 36–38 (1978).
- [20] Steven L. Detweiler, “Pulsar timing measurements and the search for gravitational waves,” *Astrophys. J.* **234**, 1100–1104 (1979).
- [21] R. S. Foster and D. C. Backer, “Constructing a Pulsar Timing Array,” *Astrophys. J.* **361**, 300 (1990).
- [22] Andrei Khmelnitsky and Valery Rubakov, “Pulsar timing signal from ultralight scalar dark matter,” *JCAP* **02**, 019 (2014), [arXiv:1309.5888 \[astro-ph.CO\]](#).
- [23] Kimihiro Nomura, Asuka Ito, and Jiro Soda, “Pulsar timing residual induced by ultralight vector dark matter,” *Eur. Phys. J. C* **80**, 419 (2020), [arXiv:1912.10210 \[gr-qc\]](#).
- [24] Yu-Mei Wu, Zu-Cheng Chen, and Qing-Guo Huang, “Pulsar timing residual induced by ultralight tensor dark matter,” *JCAP* **09**, 021 (2023), [arXiv:2305.08091 \[hep-ph\]](#).
- [25] Xiao Xue *et al.* (PPTA), “High-precision search for dark photon dark matter with the Parkes Pulsar Timing Array,” *Phys. Rev. Res.* **4**, L012022 (2022), [arXiv:2112.07687 \[hep-ph\]](#).
- [26] Juan Manuel Armaleo, Diana López Nacir, and Federico R. Urban, “Pulsar timing array constraints on spin-2 ULDM,” *JCAP* **09**, 031 (2020), [arXiv:2005.03731 \[astro-ph.CO\]](#).
- [27] David E. Kaplan, Andrea Mitridate, and Tanner Trickle, “Constraining fundamental constant variations from ultralight dark matter with pulsar timing arrays,” *Phys. Rev. D* **106**, 035032 (2022), [arXiv:2205.06817 \[hep-ph\]](#).
- [28] Nataliya K. Porayko *et al.*, “Parkes Pulsar Timing Array constraints on ultralight scalar-field dark matter,” *Phys. Rev. D* **98**, 102002 (2018), [arXiv:1810.03227 \[astro-ph.CO\]](#).
- [29] Yu-Mei Wu, Zu-Cheng Chen, Qing-Guo Huang, Xingjiang Zhu, N. D. Ramesh Bhat, Yi Feng, George Hobbs, Richard N. Manchester, Christopher J. Russell, and R. M. Shannon (PPTA), “Constraining ultralight vector dark matter with the Parkes Pulsar Timing Array second data release,” *Phys. Rev. D* **106**, L081101 (2022), [arXiv:2210.03880 \[astro-ph.CO\]](#).
- [30] Clemente Smarra *et al.* (European Pulsar Timing Array), “Second Data Release from the European Pulsar Timing Array: Challenging the Ultralight Dark Matter Paradigm,” *Phys. Rev. Lett.* **131**, 171001 (2023), [arXiv:2306.16228 \[astro-ph.HE\]](#).
- [31] Adeela Afzal *et al.* (NANOGrav), “The NANOGrav 15 yr Data Set: Search for Signals from New Physics,” *Astrophys. J. Lett.* **951**, L11 (2023), [Erratum: *Astrophys. J. Lett.* 971, L27 (2024), Erratum: *Astrophys. J.* 971, L27 (2024)], [arXiv:2306.16219 \[astro-ph.HE\]](#).
- [32] Gary P. Centers *et al.*, “Stochastic fluctuations of bosonic dark matter,” *Nature Commun.* **12**, 7321 (2021), [arXiv:1905.13650 \[astro-ph.CO\]](#).
- [33] Thibault Damour and John F. Donoghue, “Equivalence Principle Violations and Couplings of a Light Dilaton,” *Phys. Rev. D* **82**, 084033 (2010), [arXiv:1007.2792 \[gr-qc\]](#).
- [34] J. Antoniadis *et al.* (EPTA), “The second data release from the European Pulsar Timing Array - I. The dataset and timing analysis,” *Astron. Astrophys.* **678**, A48 (2023), [arXiv:2306.16224 \[astro-ph.HE\]](#).
- [35] L. Lentati *et al.*, “European Pulsar Timing Array Limits On An Isotropic Stochastic Gravitational-Wave Background,” *Mon. Not. Roy. Astron. Soc.* **453**, 2576–2598 (2015), [arXiv:1504.03692 \[astro-ph.CO\]](#).
- [36] Zaven Arzoumanian *et al.* (NANOGrav), “The NANOGrav Nine-year Data Set: Observations, Arrival Time Measurements, and Analysis of 37 Millisecond Pulsars,” *Astrophys. J.* **813**, 65 (2015), [arXiv:1505.07540 \[astro-ph.IM\]](#).
- [37] Ryan M. Shannon and James M. Cordes, “Assessing the Role of Spin Noise in the Precision Timing of Millisecond Pulsars,” *Astrophys. J.* **725**, 1607–1619 (2010), [arXiv:1010.4794 \[astro-ph.SR\]](#).
- [38] M. J. Keith *et al.*, “Measurement and correction of variations in interstellar dispersion in high-precision pulsar timing,” *Mon. Not. Roy. Astron. Soc.* **429**, 2161 (2013), [arXiv:1211.5887 \[astro-ph.GA\]](#).
- [39] J. Antoniadis *et al.* (EPTA, InPTA:), “The second data release from the European Pulsar Timing Array - III. Search for gravitational wave signals,” *Astron. Astrophys.* **678**, A50 (2023), [arXiv:2306.16214 \[astro-ph.HE\]](#).
- [40] Justin A. Ellis, Michele Vallisneri, Stephen R. Taylor, and Paul T. Baker, “Enterprise: Enhanced numerical

- toolbox enabling a robust pulsar inference suite,” Zenodo (2020).
- [41] Stephen R. Taylor, Paul T. Baker, Jeffrey S. Hazboun, Joseph Simon, and Sarah J. Vigeland, “enterprise_extensions,” (2021), v2.2.0.
- [42] Bradley P. Carlin and Siddhartha Chib, “Bayesian model choice via markov chain monte carlo methods,” *Journal of the Royal Statistical Society. Series B (Methodological)* **57**, 473–484 (1995).
- [43] Sonke Hee, Will Handley, Mike P. Hobson, and Anthony N. Lasenby, “Bayesian model selection without evidences: application to the dark energy equation-of-state,” *Mon. Not. Roy. Astron. Soc.* **455**, 2461–2473 (2016), arXiv:1506.09024 [astro-ph.CO].
- [44] Stephen R. Taylor, Rutger van Haasteren, and Alberto Sesana, “From Bright Binaries To Bumpy Backgrounds: Mapping Realistic Gravitational Wave Skies With Pulsar-Timing Arrays,” *Phys. Rev. D* **102**, 084039 (2020), arXiv:2006.04810 [astro-ph.IM].
- [45] Justin Ellis and Rutger van Haasteren, “jellis18/ptmcmcsampler: Official release,” (2017).
- [46] A. Hees, J. Guéna, M. Abgrall, S. Bize, and P. Wolf, “Searching for an oscillating massive scalar field as a dark matter candidate using atomic hyperfine frequency comparisons,” *Phys. Rev. Lett.* **117**, 061301 (2016), arXiv:1604.08514 [gr-qc].
- [47] Kyle Beloy *et al.* (BACON), “Frequency ratio measurements at 18-digit accuracy using an optical clock network,” *Nature* **591**, 564–569 (2021), arXiv:2005.14694 [physics.atom-ph].
- [48] Joel Bergé, Philippe Brax, Gilles Métris, Martin Pernot-Borràs, Pierre Touboul, and Jean-Philippe Uzan, “MICROSCOPE Mission: First Constraints on the Violation of the Weak Equivalence Principle by a Light Scalar Dilaton,” *Phys. Rev. Lett.* **120**, 141101 (2018), arXiv:1712.00483 [gr-qc].
- [49] Tanmay Kumar Poddar, Subhendra Mohanty, and Soumya Jana, “Vector gauge boson radiation from compact binary systems in a gauged $L_\mu - L_\tau$ scenario,” *Phys. Rev. D* **100**, 123023 (2019), arXiv:1908.09732 [hep-ph].
- [50] Jeff A. Dror, Ranjan Laha, and Toby Opferkuch, “Probing muonic forces with neutron star binaries,” *Phys. Rev. D* **102**, 023005 (2020), arXiv:1909.12845 [hep-ph].
- [51] Colin J. Kennedy, Eric Oelker, John M. Robinson, Tobias Bothwell, Dhruv Kedar, William R. Milner, G. Edward Marti, Andrei Derevianko, and Jun Ye, “Precision Metrology Meets Cosmology: Improved Constraints on Ultralight Dark Matter from Atom-Cavity Frequency Comparisons,” *Phys. Rev. Lett.* **125**, 201302 (2020), arXiv:2008.08773 [physics.atom-ph].
- [52] Stephan Schlamminger, K. Y. Choi, T. A. Wagner, J. H. Gundlach, and E. G. Adelberger, “Test of the equivalence principle using a rotating torsion balance,” *Phys. Rev. Lett.* **100**, 041101 (2008), arXiv:0712.0607 [gr-qc].
- [53] Hidetoshi Omiya, Kimihiro Nomura, and Jiro Soda, “Hellings-Downs curve deformed by ultralight vector dark matter,” *Phys. Rev. D* **108**, 104006 (2023), arXiv:2307.12624 [astro-ph.CO].
- [54] Rong-Gen Cai, Jing-Rui Zhang, and Yun-Long Zhang, “Angular correlation and deformed Hellings-Downs curve from spin-2 ultralight dark matter,” *Phys. Rev. D* **110**, 044052 (2024), arXiv:2402.03984 [gr-qc].